THE JOURNAL OF BIOLOGICAL CHEMISTRY VOL. 285, NO. 46, pp. 36199–36206, November 12, 2010

AMP-activated Protein Kinase Mediates Apoptosis in Response to Bioenergetic Stress through Activation of the Pro-apoptotic Bcl-2 Homology Domain-3-only Protein BMF*

Received for publication, April 26, 2010, and in revised form, August 26, 2010 Published, JBC Papers in Press, September 14, 2010, DOI 10.1074/jbc.M110.138107

Seán M. Kilbride[‡1], Angela M. Farrelly[§1], Caroline Bonner[‡], Manus W. Ward[‡], Kristine C. Nyhan[§], Caoimhín G. Concannon[‡], Claes B. Wollheim[¶], Maria M. Byrne[§], and Jochen H. M. Prehn[‡2]

From the [‡]Department of Physiology and Medical Physics, Royal College of Surgeons in Ireland, 123 St. Stephen's Green, Dublin 2, Ireland, the [§]Mater Misericordiae Hospital, Eccles Street, Dublin 7, Ireland, and the [¶]Department of Cell Physiology and Metabolism, University Medical Center, CH-1211 Geneva, Switzerland

Heterozygous loss-of-function mutations in the hepatocyte nuclear factor 1A (*HNF1A*) gene result in the pathogenesis of maturity-onset diabetes-of-the-young type 3, (HNF1A-MODY). This disorder is characterized by a primary defect in metabolism-secretion coupling and decreased beta cell mass, attributed to excessive beta cell apoptosis. Here, we investigated the link between energy stress and apoptosis activation following HNF1A inactivation. This study employed single cell fluorescent microscopy, flow cytometry, gene expression analysis, and gene silencing to study the effects of overexpression of dominant-negative (DN)-HNF1A expression on cellular bioenergetics and apoptosis in INS-1 cells. Induction of DN-HNF1A expression led to reduced ATP levels and diminished the bioenergetic response to glucose. This was coupled with activation of the bioenergetic stress sensor AMP-activated protein kinase (AMPK), which preceded the onset of apoptosis. Pharmacological activation of AMPK using aminoimidazole carboxamide ribonucleotide (AICAR) was sufficient to induce apoptosis in naive cells. Conversely, inhibition of AMPK with compound C or AMPKα gene silencing protected against DN-HNF1A-induced apoptosis. Interestingly, AMPK mediated the induction of the pro-apoptotic Bcl-2 homology domain-3-only protein Bmf (Bcl-2-modifying factor). Bmf expression was also elevated in islets of DN-HNF1A transgenic mice. Furthermore, knockdown of Bmf expression in INS-1 cells using siRNA was sufficient to protect against DN-HNF1A-induced apoptosis. Our study suggests that overexpression of DN-HNF1A induces bioenergetic stress and activation of AMPK. This in turn mediates the transcriptional activation of the pro-apoptotic Bcl-2-homology protein BMF, coupling prolonged energy stress to apoptosis activation.

Heterozygous inactivating mutations in the *HNF1A* gene result in the pathogenesis of HNF1A-MODY, the most common form of monogenic diabetes in the Western world (1). The most frequent mutation of this transcription factor occurs as a frameshift within the transactivation domain, known as pro291fsinsC-HNF1A (2). The resulting phenotype displays a primary diminished glucose-stimulated insulin secretion response and reduced beta cell mass, with patients usually presenting with symptoms during adolescence or early adulthood (1). The overexpression of dominant-negative HNF1A mutants in INS-1 cells has been a useful tool for researchers endeavoring to model HNF1A-MODY over a short period *in vitro*, and studies employing this technique have contributed significantly to elucidating the molecular targets under HNF1A control (2–5). It has been suggested that many of these molecular targets are defective in type 2 diabetes (6), and significant breakthroughs in the underlying genetic causes of type 2 diabetes have come from familial linkage analysis of the genes involved in HNF1A-MODY and the other MODY disorders (7).

Among the genes shown to be under the control of HNF1A are some of those involved in glycolytic and mitochondrial energy metabolism (2, 3). In particular, the expressions of the Glut2 glucose transporter and pyruvate kinase have been consistently shown to be reduced by dominant-negative suppression of HNF1A function (2, 3, 8, 9). Mitochondrial targets have also been identified, including decreased expression of the E1 subunit of 2-oxoglutarate dehydrogenase and increased levels of the uncoupling protein UCP2 (2, 3). Energy metabolism is intrinsically coupled to fuel-stimulated insulin secretion in beta cells with the intracellular ATP/ADP ratio serving as the primary messenger controlling the plasma membrane potential, which in turn regulates the insulin exocytotic machinery (10). Recent evidence indicates that mitochondrial dysfunction contributes to the impaired insulin secretion response to glucose (9), the primary defect in the pathogenesis of HNF1A-MODY.

As well as the impaired metabolism-secretion response, HNF1A-MODY is associated with decreased beta cell proliferation and increased beta cell apoptosis (5). Apoptosis is characterized by permeabilization of the outer mitochondrial membrane, the resultant release of cytochrome *c*, and the depolarization of the mitochondrial membrane potential (11). The activation of pro-apoptotic Bcl-2 protein family members Bax or Bak is a key signaling event in the initiation of this process (12). We have previously demonstrated that Bax is activated by dominant-negative suppression of HNF1A function in INS-1 cells (5). Bax/Bak activation is thought to be controlled by up-

* This work was supported by Health Research Board Grant RP/2008/14 and Science Foundation Ireland Grant 08/IN1/1949 (to J. H. M. P.), Grants RP/2004/220 and RP/2007/316 (to M. M. B.), and Swiss National Foundation Grant 32-66907.01 (to C. B. W.).

[1] Both authors contributed equally to this work.

[2] To whom correspondence should be addressed: Royal College of Surgeons in Ireland, 123 St. Stephen's Green, Dublin 2, Ireland. Tel.: 353-1-402-2255; Fax: 353-1-402-2447; E-mail: prehn@rcsi.ie.

regulation and/or post-translational activation of Bcl-2 homology domain-3 (BH3)[3]-only proteins (13). To date, the BH3-only protein(s), which mediate Bax activation following DN-HNF1A-induced apoptosis, have not been identified.

Although much work has focused on elucidating the role of DN-HNF1A-induced bioenergetic dysfunction in the impaired insulin secretion response, the effects of DN-HNF1A-induced bioenergetic stress on cell survival have not been examined. In this context, we here demonstrate that expression of DN-HNF1A led to ATP depletion, bioenergetic dysfunction, and activation of the bioenergetic stress sensor, AMP-activated protein kinase (AMPK). We identified the pro-apoptotic BH3-only protein Bmf as the primary mediator of DN-HNF1A-induced apoptosis, and we related AMPK activation to increased Bmf expression. This study suggests that in addition to leading to a diminished insulin secretion response to glucose, bioenergetic dysfunction results in beta cell apoptosis in HNF1A-MODY.

EXPERIMENTAL PROCEDURES

Cell Culture—INS-1 cells derived from rat insulinoma stably transfected overexpressing wild-type HNF1A (WT-HNF1A) or a dominant-negative sm6 mutant of HNF1A (DN-HNF1A) under the control of a doxycycline-dependent transcriptional activator were generated as described previously (3). The SM6 mutant gene contains 83 amino acid substitutions in the DNA-binding domain of HNF1A, which forms nonfunctional heterodimers with wild-type HNF-1A (14). Cells were cultured in RPMI 1640 medium supplemented with 10% FBS, 2 mmol/liter L-glutamine, 1 mmol/liter pyruvate, penicillin (100 units/ml), streptomycin (100 μg/ml), 10 mmol/liter HEPES, pH 7.4, and 50 μmol/liter 2-mercaptoethanol. For experiments, cells were seeded at a density of 5×10^4 cells/cm^2 for 48 h prior to treatment and were cultured in RPMI 1640 medium containing 6 mmol/liter glucose and co-treated with reagents as indicated.

Western Blotting—Following treatments cells were lysed in buffer (62.5 mmol/liter Tris-HCl, pH 6.8, 2% SDS (w/v), 10% glycerin (w/v), and protease inhibitors), and samples were boiled at 95 °C for 5 min. Protein concentration was determined using the Pierce BCA micro protein assay kit, and equal amounts (20–50 μg) were separated on 5–15% SDS-polyacrylamide gels (w/v) and blotted to nitrocellulose membranes (Protean BA 85, Schleicher & Schuell). Blots were probed with the following primary antibodies: goat polyclonal antibody to HNF1A (Santa Cruz Biotechnology), diluted 1:1000; mouse monoclonal β-actin antibody (clone DM 1A; Sigma), diluted 1:5000; rabbit polyclonal phospho(Thr-172) AMPK antibody (Cell Signaling Technology) diluted 1:1000; rabbit polyclonal AMPK antibody (Cell Signaling Technology) diluted 1:1000; rabbit polyclonal antibody to cleaved caspase 3 (Cell Signaling Technology), diluted 1:1000; rabbit polyclonal antibody to Bmf (Cell Signaling Technology), diluted 1:1000. Secondary antibodies conjugated to horseradish peroxidase were diluted 1:1000 (Pierce). Bands were detected using SuperSignal West Pico chemiluminescent substrate (Pierce) and imaged using a FujiFilm LAS-3000 imaging system (Fuji, Sheffield, UK). Images were quantified using Image J 1.41o. Briefly, the integrated intensity of each band was measured, and the intensities of background regions of the same size on the gel were subtracted. The ratio of intensity of the protein of interest was divided by the intensity of β-actin in the respective lane.

Real Time Quantitative RT-PCR—Total RNA was extracted using the RNeasy mini kit (Qiagen). First strand cDNA synthesis was performed using 1.5 μg of total RNA as template. Reverse transcription was achieved using Superscript II (Invitrogen) primed with 50 pmol of random hexamers (New England Biolabs, Ipswich, MA). Real time PCR was performed on the LightCycler 2.0 (Roche Diagnostics) using the QuantiTech SYBR Green PCR kit (Qiagen). Sense and antisense primer sequences were as follows: CAATTTCATCATCGCCCTCT and GTCTCTGATGACCCCAGGAA for *glut2*; GAGACGCTGTCCTGGAGTCA and GGCCTTGTCTTCCTGGCTTA for *bmf*; AGGCACTGCAACACAGATGC and GGAAGGAACTCAACGCTGTACG for *bad*; CCAGCTGACTGCCCTGTCTA and AGCAACTTCACCTGCTGTGC for *bim*; ATGGACTCAGCATCGGAAGG and TGGCTCATTTGCTCTTCACG for *puma*; and AGCCATCCAGGCTGTGTTGT and CAGCTGTGGTGGTGAAGCTG for β-actin. All samples were normalized to β-actin, and the data were analyzed using the Lightcycler software 4.0.

ATP Assay—Cells were treated in 24-well plates before aspiration of media and addition of 200 μl of hypotonic lysis buffer (Tris acetate buffer, pH 7.75), and samples were immediately stored at −80 °C. ATP measurements were performed using the ENLITEN ATP assay system bioluminescence detection kit (Promega, Southampton, UK) as per the manufacturer's instructions. Luminescence was recorded using a Tecan GENios in luminescence mode. ATP content values were corrected for protein concentration (determined using the Pierce BCA micro protein assay kit) and normalized to untreated control samples.

Fluorescence Microscopy/Immunohistochemistry—Cells (2×10^5) were seeded on Willco (Willco Wells, Amsterdam, Netherlands) dishes (1 cm diameter) and mounted on a thermostatically regulated stage set to 37 °C. Time lapse imaging was performed on a Zeiss Axiovert 200 M inverted microscope, and NAD(P)H autofluorescence and TMRM fluorescence were observed through a 63×, 1.4 numerical aperture oil-immersion objective lens (Zeiss). Excitation and emission wavelengths were as follows: NAD(P)H, excitation 375 ± 25 nm and emission 448 ± 32 nm; TMRM, excitation 530 ± 21 nm and emission, 592 ± 22 nm; filters and dichroic mirrors were made by Semrock (Rochester, NY). Emission and bright field images were recorded using a cooled EM CCD camera (Ixon BV 887-DCS; Andor, Belfast, Ireland). The imaging setup was controlled by MetaMorph 6.3r2, and images were analyzed using the same software as described previously (15). Images were captured at 2-min intervals. Cells were preincubated for 1 h with TMRM (20 mmol/liter) or in experimental buffer (120 mmol/liter NaCl, 3.5 mmol/liter KCl, 0.4 mmol/liter KH_2PO_4, 20 mmol/liter HEPES, 5 mmol/liter $NaHCO_3$, 1.2 mmol/liter

[3] The abbreviations used are: BH3, Bcl-2 homology domain-3; AMPK, AMP-activated protein kinase; AICAR, aminoimidazole carboxamide ribonucleotide; DN, dominant-negative; PI, propidium iodide; TMRM, tetramethylrhodamine methyl ester.

Na_2SO_4, 1.2 mmol/liter $CaCl_2$, 1.2 mmol/liter $MgCl_2$, and 6 mmol/liter glucose, pH 7.4).

For Hoechst staining of nuclear chromatin, cells were stained with Hoechst 33258 (Sigma) at a final concentration of 1 μg/ml. After incubation for 20 min at 37 °C, nuclear morphology was observed using an Eclipse TE 300 inverted microscope (Nikon, Düsseldorf, Germany) and a 20× dry objective. For each treatment, cells were analyzed for apoptotic nuclear morphology in three image subfields of each culture. Condensed and/or fragmented nuclei were scored as apoptotic nuclei and expressed as a percentage of the total population. Where cells were transfected with a plasmid expressing copGFP, only the copGFP-positive cells were analyzed.

For immunohistochemistry experiments, pancreatic sections were obtained from rat insulin promoter-DN-HNF1A and control wild-type C57BL/6JBomTac mice, the generation and genotyping of which have been previously described (16). The slices were first deparaffinized and incubated overnight at 4 °C with rabbit polyclonal Bmf antibody diluted 1:20 (Cell Signaling Technology). Slides were incubated at room temperature for 1 h with an Alexa 568-conjugated anti-rabbit antibody (1:200, Molecular Probes). The following day, the slides were stained with guinea pig anti-insulin antibody (1:20, Dako Diagnostics, Ireland) and incubated overnight at 4 °C. Following this, slides were incubated for 1 h at room temperature in FITC-labeled anti-guinea pig secondary antibody (1:200, Dako Diagnostics Ireland). Images were acquired on a Zeiss LSM510 confocal microscope (Carl Zeiss, Jena, Germany). FITC was excited at 488 nm with an argon laser (1%), and the emission was collected through a 505–550-nm barrier filter. Alexa 568 was excited at 543 nm with a helium neon laser (3%), and the emission was collected through 560-nm long pass barrier filter. Images were processed using Zeiss LSM Image Browser 3,2,0,115 (Carl Zeiss, Germany).

Plasmids, Transfections, and siRNA—Plasmids and siRNAs were transfected using DharmaFECT Duo (Dharmacon, CO) in Opti-MEM (BioSciences, Dublin, Ireland). Inhibition of AMPK expression was achieved by transiently transfecting cells with a vector expressing siRNA targeting $\alpha 1/\alpha 2$ AMPK, while control samples were transfected with a scrambled sequence, as described previously (17, 18). Silencing of Bmf expression was performed utilizing siRNA duplexes purchased from Sigma Proligo (Paris, France). Sequences were as follows: sense, CCAGAAAGCUUCAGUGCAUdTdT; antisense, AUGCACUGAAGCUUUCUGGdTdT.

Flow Cytometry—Cells were harvested with trypsin-EDTA and washed with PBS. Cells were resuspended in binding buffer (10 mmol/liter HEPES, 135 mmol/liter NaCl, 5 mmol/liter $CaCl_2$) containing annexin V-FITC conjugate and propidium iodide (Biovision, Mountain View, CA), as per manufacturer's instructions, and incubated at room temperature for 15 min. Cells were analyzed using a Cyflow ML 16 flow cytometer (Partec, Münster, Germany). For all treatments, 1×10^4 cells were acquired and analyzed using the Flowmax software (Partec, Münster, Germany).

Statistics—Statistics were carried out on GraphPad InStat software using one-way analysis of variance and Student-Newman-Keuls post hoc test. Where the p value was < 0.05, groups were considered to be significantly different.

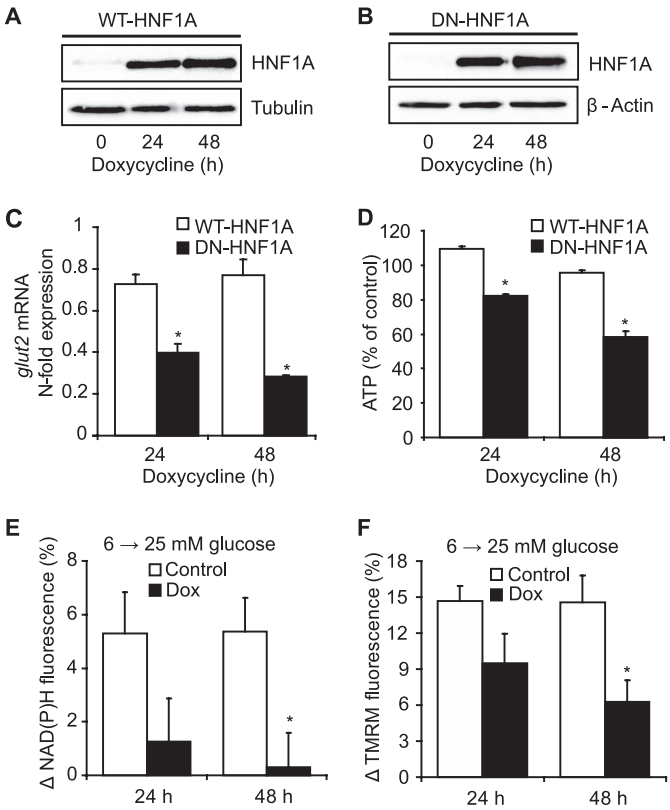

FIGURE 1. **Overexpression of DN-HNF1A causes bioenergetic stress in INS-1 cells.** Induction of WT-HNF1A (*A*) or DN-HNF1A (*B*) in response to treatment with 500 ng/ml doxycycline is shown. β-Actin levels were probed as a loading control. *C, Glut2* mRNA expression levels following induction of WT-HNF1A or DN-HNF1A for indicated times are shown. Expression levels presented were normalized to β-actin and expressed relative to untreated controls. Data shown represent mean ± S.E. from $n = 4$ cultures. *, $p < 0.05$ compared with wild-type controls. *D,* ATP levels during induction of WT-HNF1A or DN-HNF1A. ATP levels were measured as described under "Materials and Methods" and normalized to untreated controls. Data shown represent mean ± S.E. from $n = 4$ cultures. This experiment was repeated at least twice with similar results. *, $p < 0.05$ compared with untreated controls. *E,* increase in single cell NAD(P)H and TMRM fluorescence (*F*) 10 min after increasing extracellular glucose from the basal level of 6–25 mmol/liter, as monitored using single cell time-lapse microscopy. Cells were pretreated with doxycycline for 24 or 48 h where indicated. Data shown represent mean ± S.E. from $n = 32$–48 cells. *, $p < 0.05$ compared with untreated controls.

RESULTS

Expression of DN-HNF1A Causes Bioenergetic Dysfunction in INS-1 Cells—Overexpression of wild-type or dominant-negative mutant of HNF1A was induced in INS-1 cells using a tetracycline-dependent transactivator system using 500 ng/ml doxycycline for 24 and 48 h (Fig. 1, *A* and *B*). Previously, we demonstrated a reduction in expression of pyruvate kinase over this time scale after dominant-negative suppression of HNF1A function (8). Indeed, numerous other downstream target genes involved in energy metabolism have been shown to be down-regulated 24 h after suppression (9). This study correlated expression of DN-HNF1A with a significant decrease in the level of glucose transporter *glut2* mRNA (Fig. 1*C*). The downstream effects of such reductions in expression levels on beta cell bioenergetic function were examined. Intracellular ATP

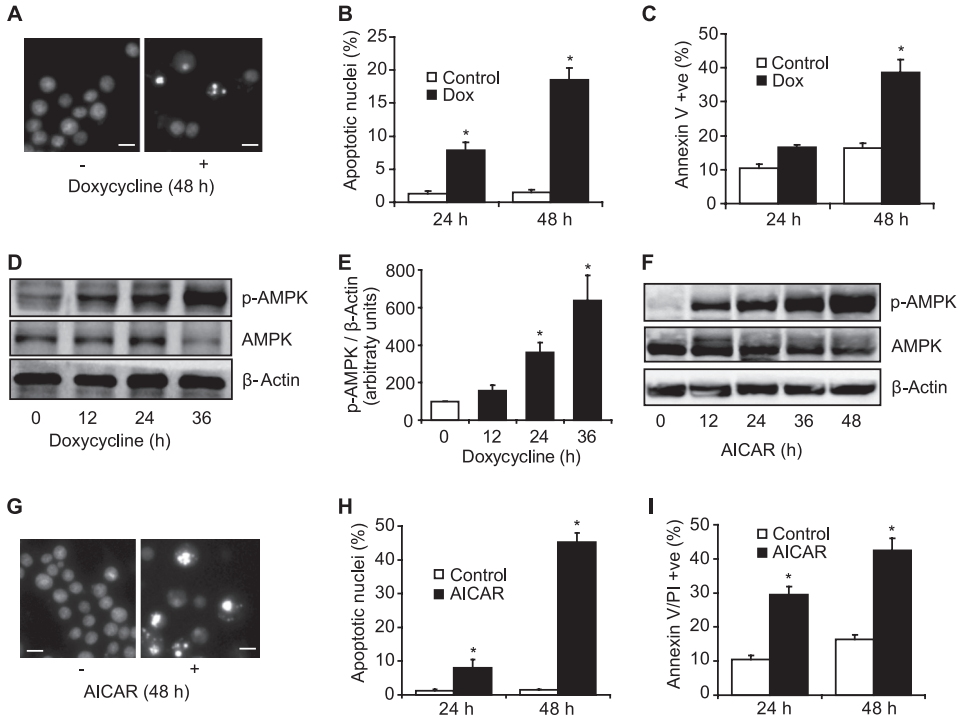

FIGURE 2. **AMPK is activated during DN-HNF1A-induced apoptosis, and activation is sufficient to induce apoptosis.** *A,* induction of apoptosis by prolonged DN-HNF1A overexpression in INS-1 cells. Nuclear morphology was assessed by Hoechst staining. *Scale bar,* 5 μm. *B,* condensed/fragmented nuclei were scored as apoptotic and expressed as a percentage of totals. Three subfields were counted per well, and data shown represent means ± S.E. from $n = 4$ cultures. This experiment was repeated twice with similar results. *, $p < 0.05$ compared with untreated controls. *C,* flow cytometry analysis of the effect DN-HNF1A overexpression on apoptosis. Cells were treated with doxycycline for the times indicated and stained with an annexin V-FITC conjugate and PI as described under "Experimental Procedures." Cell populations which were positive for annexin V or both annexin V and PI were gated and expressed as a percentage of total events. Data shown represent means ± S.E. from $n = 4$ cultures. This experiment was repeated twice with similar results. *, $p < 0.05$ compared with untreated controls. *D,* Western blot of phospho-Thr-172 AMPK and total AMPK protein levels after treatment with doxycycline for the indicated times. Probing with β-actin served as a loading control. *E,* quantification of phospho-Thr-172 AMPK levels after treatment with doxycycline for the indicated times. Western blot images were analyzed as described under "Experimental Procedures." Data shown represent means ± S.E. from three independent experiments. *, $p < 0.05$ compared with untreated controls. *F,* Western blot analysis of phospho-Thr-172 AMPK and total AMPK protein levels after treatment with the AMPK activator AICAR for the indicated times. Probing with β-actin served as a loading control. *G,* representative images of Hoechst-stained nuclei of INS-1 cells treated with AICAR (2.5 mmol/liter) or control. *Scale bar,* 5 μm. *H,* effect of AICAR on apoptosis. Cells were treated with AICAR for the times shown and stained with Hoechst. Three images were taken from each culture, and data shown represent means ± S.E. from $n = 4$ cultures. This experiment was repeated twice with similar results. *, $p < 0.05$ compared with untreated controls. *I,* flow cytometry analysis of the effect of AICAR on apoptosis. Cells were treated with AICAR for the indicated times and stained with an annexin V-FITC conjugate and PI as described above. Data shown represent means ± S.E. from $n = 4$ cultures. This experiment was repeated twice with similar results. *, $p < 0.05$ compared with untreated controls.

level was decreased by ~20% by 24 h and by 40% after 48 h (Fig. 1*D*). ATP is generated mainly by metabolism of glucose via glycolysis and mitochondrial aerobic metabolism, which relies on the maintenance of the mitochondrial membrane potential. We have previously shown that overexpression of DN-HNF1A in INS-1 cells also affects the mitochondrial membrane potential, with hyperpolarization prominent after 24 h, followed by depolarization in most cells by 48 h (5).

Insulin secretion from beta cells is mediated by the bioenergetic response to secretagogues, and the increased ATP level in response to increased extracellular glucose has been well characterized (2, 3, 10). The ATP response to glucose in INS-1 cells is diminished by dominant-negative suppression of HNF1A function, with mitochondrial dysfunction thought to contribute to this effect (9). In this study, we examined the response of NAD(P)H autofluorescence to increased extracellular glucose in single cells, and in parallel we monitored the membrane potential response using TMRM. NAD(P)H autofluorescence has been shown previously to immediately increase in INS-1 cells in response to increased extracellular glucose concentrations in the medium with concurrent hyperpolarization of mitochondrial membrane potential under these conditions (19). Indeed, we observed increased NAD(P)H autofluorescence within 10 min following glucose stimulation, an effect that was shown to be abolished in cells expressing DN-HNF1A for 48 h (Fig. 1*E*). The TMRM response to high glucose showed an immediate increase in fluorescence, indicative of hyperpolarization, and which was similarly diminished in cells expressing DN-HNF-1A for 48 h (Fig. 1*F*). In summary, these data allowed us to conclude that bioenergetic failure becomes prominent after 24–48 h of DN-HNF1A induction.

AMPK Mediates DN-HNF1A-induced Apoptosis—We have previously demonstrated that dominant-negative inactivation of HNF1A function triggers apoptosis in INS-1 cells (5). In this study, the induction of apoptosis was quantified using Hoechst staining of nuclei (Fig. 2*A*). The percentage of nuclei that was were condensed and fragmented (apoptotic) was found to be significantly increased after a 24-h induction of DN-HNF1A and was further increased after 48 h (Fig. 2*B*). The translocation of the membrane phospholipid phosphatidylserine from the inner to the outer leaflet of the plasma membrane was considered to be an earlier marker of apoptosis than the changes in nuclear morphology (20) and was quantified by flow cytometry using an annexin V/fluorescein isothiocyanate (FITC) conjugate and propidium iodide (PI). Apoptosis was also shown to be increased by this method after a 48-h induction of DN-HNF1A (Fig. 2*C*).

To investigate the relationship between cellular stress induced by energy depletion and apoptosis in our model, we examined the activation of the bioenergetic stress sensor AMPK. AMPK is activated in response to the reduced ATP:AMP ratio and acts to reduce ATP consumption by switching the primary means of generating ATP to catabolism in times of energy stress (21). Phosphorylated AMPK is the activated form and is increased in numerous cell types in response to bioenergetic dysfunction (22). Chronic activation of AMPK has previ-

ously been shown to induce apoptosis in primary beta cells (23) and in an insulin-secreting beta cell line (24). Therefore, we investigated the level of phosphorylated AMPK (p-AMPK) following DN-HNF1A induction. The level of phosphorylated AMPK was significantly increased by induction of DN-HNF1A for 24 and 36 h (Fig. 2, *D* and *E*). Furthermore, activation of AMPK using the pharmacological agonist AICAR in naive INS-1 cells resulted in a time-dependent increase in p-AMPK (Fig. 2*F*), which interestingly was coupled to increased levels of apoptosis as assessed after 24 and 48 h of AICAR treatment (Fig. 2, *G–I*).

Because AMPK was activated during DN-HNF1A-induced apoptosis, and AMPK activation *per se* was sufficient to induce apoptosis, we investigated the effect of inhibition of AMPK activity on DN-HNF1A-induced apoptosis. To this end, we first pharmacologically inhibited AMPK activity using compound C and examined its effects on phosphorylated AMPK and cleaved caspase 3 by Western blot. Caspase 3 is cleaved to become active, which is considered to be a primary event in the initiation of apoptosis. Compound C was found to inhibit DN-HNF1A-induced activation of AMPK (Fig. 3, *A* and *B*), which correlated with decreased levels of DN-HNF1A-induced cleaved caspase 3 (Fig. 3, *C* and *D*). Furthermore, the level of DN-HNF1A-induced apoptosis after 48 h was dramatically attenuated in cells co-treated with compound C (Fig. 3*E*). To ensure that the protective effects observed using compound C were not due to possible off-target effects, we utilized siRNA technology to silence AMPK expression, which we have previously used to effectively target the $\alpha 1/\alpha 2$ subunit (17). As demonstrated in Fig. 3*F*, siRNA knockdown of AMPK was also shown to be protective against DN-HNF1A-induced apoptosis (Fig. 3*F*).

Overexpression of DN-HNF1A Induces AMPK-mediated Bmf Up-regulation—We have already established that dominant-negative suppression of HNF1A function initiates cell death via the mitochondrial apoptosis pathway, which is regulated by pro-apoptotic proteins within the Bcl-2 family of BH3-only proteins, including Bmf, Bad, Puma, and Bim (25). To investigate the potential role of these proteins in DN-HNF1A-induced apoptosis, we performed quantitative PCR analysis of their mRNA levels 24 and 48 h after DN-HNF1A induction. As demonstrated in Fig. 4*A*, *bmf* mRNA was most prominently up-regulated, showing a 3-fold increase in mRNA levels 24 h after treatment and a >6-fold increase at 48 h (Fig. 4*A*). This was confirmed at the protein level with increased Bmf levels following overexpression of DN-HNF1A but not WT-HNF1A (Fig. 4, *B* and *C*). Because dominant-negative suppression of HNF1A function increased AMPK activity and resulted in increased *bmf* expression, we next examined the effects of AMPK activity on Bmf levels. Activation of AMPK with AICAR for 24 h increased Bmf protein expression (Fig. 4, *D* and *E*). Conversely, inhibition of DN-HNF1A-induced AMPK activation with compound C diminished the Bmf induction (Fig. 4, *F* and *G*). Taken together, these data suggest that DN-HNF1A-induced Bmf expression is mediated in an AMPK-dependent manner.

Role of Bmf in DN-HNF1A-induced Apoptosis—It has previously been demonstrated that transgenic mice engineered to express DN-HNF1A in beta cells display a HNF1A-MODY-like

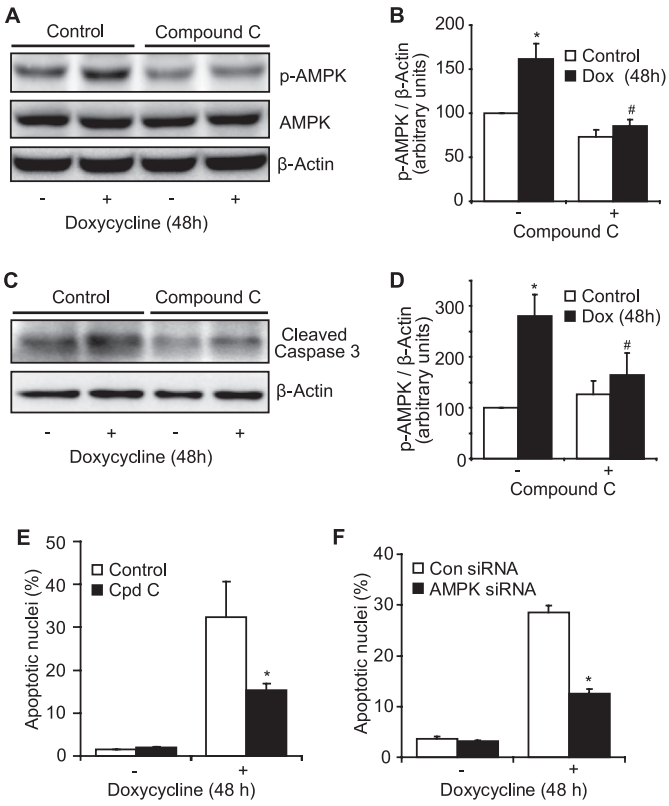

FIGURE 3. **AMPK mediates DN-HNF1A-induced apoptosis.** *A,* Western blot of phospho-Thr-172 AMPK levels after treatment with doxycycline in the presence and absence of the AMPK inhibitor compound C (20 μM) for 48 h. *B,* quantification of phospho-Thr-172 AMPK levels after treatment with doxycycline for indicated times. Western blot images were analyzed as described under "Experimental Procedures." Data shown represent means ± S.E. from three independent experiments. *, $p < 0.05$ compared with untreated controls. #, $p < 0.05$ compared with samples treated with doxycycline alone. *C,* Western blot of cleaved caspase 3 levels after treatment with doxycycline in the presence and absence of compound C (20 μM) for the indicated times. *D,* quantification of cleaved caspase 3 levels after treatment with doxycycline for the indicated times. Western blot images were analyzed as described under "Experimental Procedures." Data shown represent means ± S.E. from three independent experiments. *E,* effect of compound C on DN-HNF1A-induced apoptosis. Cells were treated with doxycycline and/or compound C as indicated for 48 h and then stained with Hoechst. Three images were taken from each culture, and the number of cells with apoptotic nuclei was quantified. Data shown represent means ± S.E. from $n = 4$ cultures. This experiment was repeated twice with similar results. *, $p < 0.05$ compared with samples treated with doxycycline alone. *F,* effect of AMPK gene silencing on DN-HNF1A-induced apoptosis. Cells were transiently transfected with a copGFP-expressing vector containing a scrambled or *AMPK* siRNA sequence and subsequently treated with doxycycline and as indicated for the times shown. Approximately 35% of cells were found to be copGFP-positive. Cultures were stained with Hoechst, and three images were taken from each well. Fragmented and/or condensed nuclei in copGFP-positive cells were scored as apoptotic and expressed as a percentage of total copGFP-positive cells. Data shown represent means ± S.E. from $n = 4$ cultures. *, $p < 0.05$ compared with samples transfected with control siRNA and treated with doxycycline for 48 h.

phenotype, including impaired glucose-stimulated insulin secretion and evidence of beta cell apoptosis (16). Immunostaining of pancreatic slices from these mice also revealed increased levels of Bmf within islets, compared with wild-type controls (Fig. 5*A*). We next investigated the effect of gene silencing of *bmf* expression on DN-HNF1A-induced apoptosis. This was achieved by transiently transfecting with *bmf* siRNA prior to DN-HNF1A induction. The DN-HNF1A-induced up-regulation of the Bmf protein was prevented in Bmf

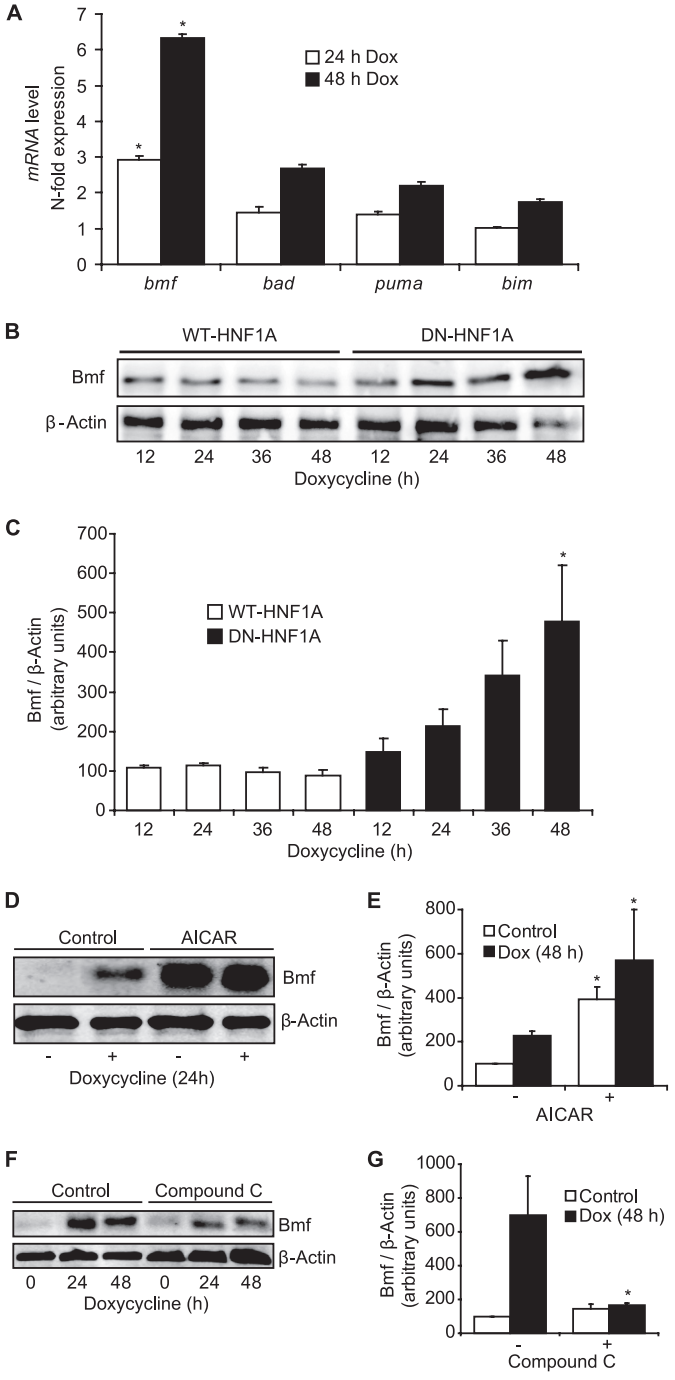

FIGURE 4. **DN-HNF1A induces an AMPK-dependent increase in Bmf expression.** *A,* real time quantitative PCR analysis of the expression levels of *bmf, bad, puma,* and *bim* mRNA after induction of DN-HNF1A for 24 or 48 h. Expression levels presented were normalized to β-actin and expressed relative to untreated controls. Data shown represent means ± S.E. from $n = 4$ cultures. *, $p < 0.05$ compared with untreated controls. *B,* time course of Bmf protein levels after treatment with doxycycline as determined by Western blotting. Cells were induced to overexpress either WT-HNF1A or DN-HNF1A for the times indicated. Probing with β-actin served as a loading control. *C,* quantification of Bmf protein levels after treatment with doxycycline for the indicated times. Western blot images were analyzed as described under "Experimental Procedures." Data shown represent means ± S.E. from three independent experiments. *, $p < 0.05$ compared with untreated controls. *D,* Western blot of Bmf levels after treatment with doxycycline in the presence and absence of AICAR for 24 h. β-Actin levels were probed as a loading control. *E,* quantification of Bmf protein levels after treatment with doxycycline and/or AICAR as indicated for 24 h. Western blot images were analyzed as described under "Experimental Procedures." Data shown represent means ± S.E. from three independent experiments. *, $p < 0.05$ compared with untreated controls. *F,* Western blot of Bmf levels after DN-HNF1A induction in the presence and absence of compound C (20 μM) as shown for the indicated times. Probing with β-actin served as a loading control. *G,* quantification of Bmf protein levels after treatment with doxycycline and/or compound C as indicated for 48 h. Western blot images were analyzed as described under "Experimental Procedures." Data shown represent means ± S.E. from at least three independent experiments. *, $p < 0.05$ compared with untreated controls.

siRNA-transfected samples compared with those transfected with scrambled siRNA (Fig. 5*B*). Consistent with the inhibition of *bmf* expression, DN-HNF1A induced apoptosis was severely attenuated in *bmf* siRNA-transfected cells compared with control siRNA-transfected cells (Fig. 5, *C* and *D*).

DISCUSSION

DN-HNF1A-induced bioenergetic dysfunction in pancreatic beta cells has previously been examined in the context of diminished insulin response to glucose stimulation (3, 5). In this study, we demonstrate that the bioenergetic stress sensor AMPK is activated early after dominant-negative suppression of HNF1A function. Furthermore, AMPK activation is both necessary and sufficient to induce cell death. We identified Bmf as the primary pro-apoptotic BH3-only protein responsible for initiating AMPK-mediated DN-HNF1A-induced apoptosis, thereby linking prolonged bioenergetic stress to the activation of apoptosis.

We have previously demonstrated that overexpression of DN-HNF1A in INS-1 cells triggers apoptosis via the mitochondrial pathway, as shown by cytochrome *c* release and caspase 9 and 3 activation (5). Here, we demonstrate that ATP levels are reduced by dominant-negative suppression of HNF1A function, correlating with an increase in AMPK activity. AMPK is a serine/threonine kinase that is activated by phosphorylation during ATP-depleting conditions and is central to the maintenance of cellular energy homeostasis (26, 27). Upstream kinases include the tumor suppressor LKB1 kinase (28), calmodulin kinase kinase β (CaMKKβ) (29), and transforming growth factor β-activated kinase (TAK1) (30). Activation has been shown to stimulate catabolism and inhibit fatty acid and cholesterol synthesis, with the net effect of reducing ATP consumption and promoting anaerobic ATP synthesis (21). AMPK activation has also been implicated in promoting cell survival by regulating macroautophagy (31, 32).

The sensitivity of AMPK activity to energy conditions within cells as well as the ability of AMPK to regulate energy metabolism have made it the subject of much recent diabetes research (33). Although AMPK activation may initially promote cell survival by enhancing ATP generation, this study demonstrates that prolonged AMPK activation during DN-HNF1A induction or pharmacological activation of AMPK with AICAR induces INS-1 cell apoptosis. Indeed, previous studies have demonstrated that prolonged activation of AMPK results in beta cell apoptosis in insulinoma cells (23) and in isolated islets (35). Moreover, transplantation of islets expressing a constitutively active form of AMPK to streptozotocin-induced diabetic mice resulted in a reduced level of beta cell survival compared with control syngeneic islets, whereas those expressing a dominant-

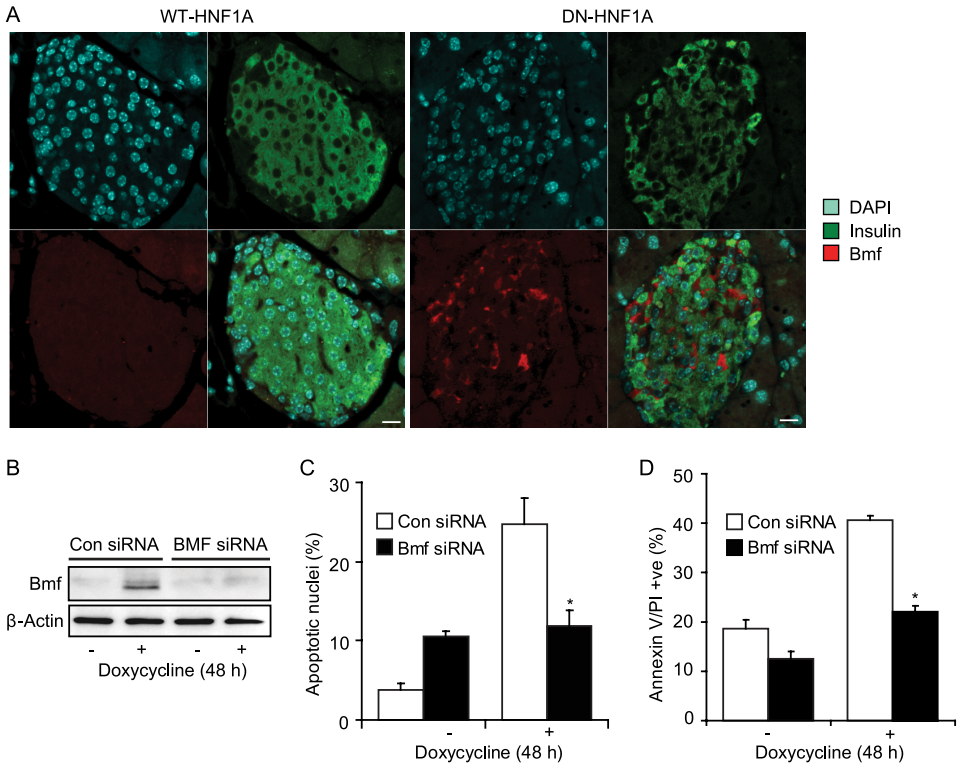

FIGURE 5. **DN-HNF1A-induced apoptosis is mediated by Bmf.** *A,* immunostaining of paraffin-embedded pancreatic slices showing islets isolated from WT-HNF1A C57BL/6JBomTac mice or rat insulin promoter-DN-HNF1A transgenic mice. Islets are differentiated from surrounding pancreatic tissue by the expression of relatively high levels of insulin, shown here in *green*. Bmf staining is shown in *red,* and the nuclei were counterstained with DAPI (*cyan*). *Scale bar,* 10 μm. *B,* Western blot of Bmf protein levels in samples transfected with control or *bmf* siRNA and subsequently treated with doxycycline for 48 h where indicated. Probing with β-actin served as a loading control. *C,* effect of reduced Bmf expression on DN-HNF1A-induced apoptosis. Cells were transfected with either a scrambled or *bmf* siRNA sequence and subsequently treated with doxycycline for 48 h. Following treatment, cultures were stained with Hoechst, and three images were taken from each well. Condensed/fragmented nuclei were scored as apoptotic and expressed as a percentage of totals. Data shown represent mean ± S.E. from $n = 4$ cultures. This experiment was repeated twice with similar results. *, $p < 0.05$ compared with control siRNA treated with doxycycline. *D,* flow cytometry analysis of the effect of *bmf* gene silencing on DN-HNF1A-induced apoptosis. Cells were then harvested and co-stained with an annexin V-FITC conjugate and PI as described under "Experimental Procedures." Cell populations that were positive for annexin V or both annexin V and PI were gated and expressed as a percentage of total events. Data shown represent mean ± S.E. from $n = 4$ cultures. This experiment was repeated twice with similar results. *, $p < 0.05$ compared with control siRNA treated with doxycycline.

negative form of AMPK improved graft efficiency (34). Later, it was demonstrated using an insulinoma cell line that a cytokine-induced reduction in ATP level was followed by apoptosis and that overexpression of DN-AMPK protected against cell death in this model (35). In this study, we show that DN-HNF1A reduces ATP and also induces AMPK-dependent apoptosis, which can be attenuated by inhibition of AMPK with compound C.

The role of AMPK as a potential therapeutic target for the treatment of diabetes has thus been explored (36). Biguanides such as metformin, currently one of the most frequently prescribed pharmacological treatments for type 2 diabetes, are known to control plasma glucose levels via AMPK activation, promoting glucose utilization in skeletal muscle and reducing hepatic gluconeogenesis (37). However, metformin-induced chronic AMPK activation can diminish insulin synthesis and secretion in beta cells, causing apoptosis (38, 39). Nevertheless, metformin-induced apoptosis was only observed at concentrations that exceeded those that are clinically relevant, and metformin treatment has been shown to remain effective in several long term follow up studies (40, 41). Collectively, these data suggest that although physiological or pharmacological activation of AMPK can have beneficial effects on energy regulation in individual cells or at an organ or whole-body level, it may also be detrimental to beta cell function and survival when prolonged or uncompensated.

The molecular mechanisms of how prolonged AMPK activation induces apoptosis have not been fully elucidated. Kefas *et al.* (24) demonstrated that AICAR-induced apoptosis in beta cells was JNK-dependent. Apoptosis is controlled by the activity of pro- and anti-apoptotic Bcl-2 family members. Recently, our group has demonstrated that pro-apoptotic BH3-only protein expression is mediated by AMPK in a neuronal excitotoxic injury model in which JNK-dependent apoptosis occurs (42). In this study, we demonstrate that expression of DN-HNF1A induces a rather selective increase in expression of Bmf. Furthermore, we demonstrate that activation of AMPK is required and sufficient to mediate this effect. Bmf was first isolated by using the anti-apoptotic Bcl-2 family member Mcl-1 as bait and was found to contain a single BH3 domain that interacts with this and other prosurvival Bcl-2 proteins, including Bcl-2, Bcl-x_L, and Bcl-w (43). The pro-apoptotic BH3-only protein was thus named Bmf (Bcl-2-modifying factor), and it was found to also contain a dynein-binding motif, leading to the conclusion that Bmf is sequestered in healthy cells by association with the myosin V actin motor complex and mediated apoptosis when unleashed by stress signals, such as loss of cell attachment (43, 44). Later it was shown that *bmf* is also up-regulated at the mRNA level by cytoskeletal disruption and is thought to mediate apoptosis during normal tissue development (45). Here, we demonstrate a specific role of Bmf in apoptosis during energetic stress in insulin-secreting cells. *bmf* mRNA was previously shown to be down-regulated by the anti-diabetic drug pioglitazone in rat pancreatic islets exposed to palmitate, suggesting a role in apoptosis induced by diabetic lipotoxicity (46). In this study, we also show that Bmf was not detected by immunohistochemistry of pancreatic islets of adult wild-type C57BL/6JBomTac mice but was widespread throughout DN-HNF1A transgenic islets.

Importantly, gene silencing experiments demonstrated that Bmf was also required for DN-HNF1A-induced apoptosis. Bmf expression has been shown to be regulated by JNK activation in

kidney cells (47), and there is strong evidence that AMPK-induced beta cell apoptosis is also mediated by JNK activation (24). It has also been demonstrated that Bmf is negatively regulated by Akt (40), and our group has shown that DN-HNF1A decreases Akt signaling in INS-1 cells (4). Furthermore, DN-HNF1A-induced apoptosis is ameliorated by increasing Akt activity (4). Interestingly, AMPK activation decreases mammalian target of rapamycin signaling (48) and via this route may decrease Akt activation downstream of mammalian target of rapamycin.

In conclusion, this study presents compelling evidence indicating that AMPK activation mediates DN-HNF1A-induced apoptosis in a Bmf-dependent manner. Dominant-negative suppression of HNF1A function causes sufficient bioenergetic stress to activate AMPK, leading to beta cell dysfunction and apoptosis. This suggests that AMPK activation within beta cells plays a role in the pathogenesis of HNF1A-MODY, where a primary insulin secretion defect is compounded by increased apoptosis and consequently reduced beta cell mass.

Acknowledgment—We thank Heiko Düssmann, Dept. of Physiology and Medical Physics, Royal College of Surgeons in Ireland, Dublin, for technical assistance.

REFERENCES

1. Yamagata, K., Oda, N., Kaisaki, P. J., Menzel, S., Furuta, H., Vaxillaire, M., Southam, L., Cox, R. D., Lathrop, G. M., Boriraj, V. V., Chen, X., Cox, N. J., Oda, Y., Yano, H., Le Beau, M. M., Yamada, S., Nishigori, H., Takeda, J., Fajans, S. S., Hattersley, A. T., Iwasaki, N., Hansen, T., Pedersen, O., Polonsky, K. S., Bell, G. I., *et al.* (1996) *Nature* **384,** 455–458
2. Wang, H., Antinozzi, P. A., Hagenfeldt, K. A., Maechler, P., and Wollheim, C. B. (2000) *EMBO J.* **19,** 4257–4264
3. Wang, H., Maechler, P., Hagenfeldt, K. A., and Wollheim, C. B. (1998) *EMBO J.* **17,** 6701–6713
4. Wobser, H., Bonner, C., Nolan, J. J., Byrne, M. M., and Prehn, J. H. (2006) *Diabetologia* **49,** 519–526
5. Wobser, H., Düssmann, H., Kögel, D., Wang, H., Reimertz, C., Wollheim, C. B., Byrne, M. M., and Prehn, J. H. (2002) *J. Biol. Chem.* **277,** 6413–6421
6. Blumenfeld, M., Maury, M., Chouard, T., Yaniv, M., and Condamine, H. (1991) *Development* **113,** 589–599
7. Vaxillaire, M., and Froguel, P. (2006) *Endocrinol. Metab. Clin. North Am.* **35,** 371–384
8. Farrelly, A. M., Wobser, H., Bonner, C., Anguissola, S., Rehm, M., Concannon, C. G., Prehn, J. H., and Byrne, M. M. (2009) *Diabetologia* **52,** 136–144
9. Pongratz, R. L., Kibbey, R. G., Kirkpatrick, C. L., Zhao, X., Pontoglio, M., Yaniv, M., Wollheim, C. B., Shulman, G. I., and Cline, G. W. (2009) *J. Biol. Chem.* **284,** 16808–16821
10. MacDonald, M. J., Fahien, L. A., Brown, L. J., Hasan, N. M., Buss, J. D., and Kendrick, M. A. (2005) *Am. J. Physiol. Endocrinol. Metab.* **288,** E1–E15
11. Desagher, S., and Martinou, J. C. (2000) *Trends Cell Biol.* **10,** 369–377
12. Wei, M. C., Zong, W. X., Cheng, E. H., Lindsten, T., Panoutsakopoulou, V., Ross, A. J., Roth, K. A., MacGregor, G. R., Thompson, C. B., and Korsmeyer, S. J. (2001) *Science* **292,** 727–730
13. Huang, D. C., and Strasser, A. (2000) *Cell* **103,** 839–842
14. Nicosia, A., Monaci, P., Tomei, L., De Francesco, R., Nuzzo, M., Stunnenberg, H., and Cortese, R. (1990) *Cell* **61,** 1225–1236
15. Ward, M. W., Huber, H. J., Weisová, P., Düssmann, H., Nicholls, D. G., and Prehn, J. H. (2007) *J. Neurosci.* **27,** 8238–8249
16. Hagenfeldt-Johansson, K. A., Herrera, P. L., Wang, H., Gjinovci, A., Ishihara, H., and Wollheim, C. B. (2001) *Endocrinology* **142,** 5311–5320
17. Weisová, P., Concannon, C. G., Devocelle, M., Prehn, J. H., and Ward, M. W. (2009) *J. Neurosci.* **29,** 2997–3008
18. Woods, A., Azzout-Marniche, D., Foretz, M., Stein, S. C., Lemarchand, P., Ferré, P., Foufelle, F., and Carling, D. (2000) *Mol. Cell. Biol.* **20,** 6704–6711
19. Mármol, P., Pardo, B., Wiederkehr, A., del Arco, A., Wollheim, C. B., and Satrústegui, J. (2009) *J. Biol. Chem.* **284,** 515–524
20. Schutte, B., Nuydens, R., Geerts, H., and Ramaekers, F. (1998) *J. Neurosci. Methods* **86,** 63–69
21. Hardie, D. G. (2008) *Int. J. Obes.* **32,** S7–S12
22. Viollet, B., Mounier, R., Leclerc, J., Yazigi, A., Foretz, M., and Andreelli, F. (2007) *Diabetes Metab.* **33,** 395–402
23. Kefas, B. A., Heimberg, H., Vaulont, S., Meisse, D., Hue, L., Pipeleers, D., and Van de Casteele, M. (2003) *Diabetologia* **46,** 250–254
24. Kefas, B. A., Cai, Y., Ling, Z., Heimberg, H., Hue, L., Pipeleers, D., and Van de Casteele, M. (2003) *J. Mol. Endocrinol.* **30,** 151–161
25. Youle, R. J., and Strasser, A. (2008) *Nat. Rev. Mol. Cell Biol.* **9,** 47–59
26. Hardie, D. G. (2004) *J. Cell Sci.* **117,** 5479–5487
27. Hardie, D. G., Hawley, S. A., and Scott, J. W. (2006) *J. Physiol.* **574,** 7–15
28. Shaw, R. J., Kosmatka, M., Bardeesy, N., Hurley, R. L., Witters, L. A., DePinho, R. A., and Cantley, L. C. (2004) *Proc. Natl. Acad. Sci. U.S.A.* **101,** 3329–3335
29. Leclerc, I., and Rutter, G. A. (2004) *Diabetes* **53,** S67–S74
30. Momcilovic, M., Hong, S. P., and Carlson, M. (2006) *J. Biol. Chem.* **281,** 25336–25343
31. Meley, D., Bauvy, C., Houben-Weerts, J. H., Dubbelhuis, P. F., Helmond, M. T., Codogno, P., and Meijer, A. J. (2006) *J. Biol. Chem.* **281,** 34870–34879
32. Viana, R., Aguado, C., Esteban, I., Moreno, D., Viollet, B., Knecht, E., and Sanz, P. (2008) *Biochem. Biophys. Res. Commun.* **369,** 964–968
33. Viollet, B., Guigas, B., Leclerc, J., Hebrard, S., Lantier, L., Mounier, R., Andreelli, F., and Foretz, M. (2009) *Acta Physiol.* **196,** 81–98
34. Richards, S. K., Parton, L. E., Leclerc, I., Rutter, G. A., and Smith, R. M. (2005) *J. Endocrinol.* **187,** 225–235
35. Riboulet-Chavey, A., Diraison, F., Siew, L. K., Wong, F. S., and Rutter, G. A. (2008) *Diabetes* **57,** 415–423
36. Viollet, B., Lantier, L., Devin-Leclerc, J., Hebrard, S., Amouyal, C., Mounier, R., Foretz, M., and Andreelli, F. (2009) *Front. Biosci.* **14,** 3380–3400
37. Zhou, G., Myers, R., Li, Y., Chen, Y., Shen, X., Fenyk-Melody, J., Wu, M., Ventre, J., Doebber, T., Fujii, N., Musi, N., Hirshman, M. F., Goodyear, L. J., and Moller, D. E. (2001) *J. Clin. Invest.* **108,** 1167–1174
38. Kefas, B. A., Cai, Y., Kerckhofs, K., Ling, Z., Martens, G., Heimberg, H., Pipeleers, D., and Van de Casteele, M. (2004) *Biochem. Pharmacol.* **68,** 409–416
39. Leclerc, I., Woltersdorf, W. W., da Silva Xavier, G., Rowe, R. L., Cross, S. E., Korbutt, G. S., Rajotte, R. V., Smith, R., and Rutter, G. A. (2004) *Am. J. Physiol. Endocrinol. Metab.* **286,** E1023–E1031
40. Rachmani, R., Slavachevski, I., Levi, Z., Zadok, B., Kedar, Y., and Ravid, M. (2002) *Eur. J. Intern. Med.* **13,** 428
41. Kooy, A., de Jager, J., Lehert, P., Bets, D., Wulffelé, M. G., Donker, A. J., and Stehouwer, C. D. (2009) *Arch. Intern. Med.* **169,** 616–625
42. Concannon, C. G., Tuffy, L. P., Weisová, P., Bonner, H. P., Dávila, D., Bonner, C., Devocelle, M. C., Strasser, A., Ward, M. W., and Prehn, J. H. (2010) *J. Cell Biol.* **189,** 83–94
43. Puthalakath, H., Villunger, A., O'Reilly, L. A., Beaumont, J. G., Coultas, L., Cheney, R. E., Huang, D. C., and Strasser, A. (2001) *Science* **293,** 1829–1832
44. Puthalakath, H., and Strasser, A. (2002) *Cell Death Differ.* **9,** 505–512
45. Schmelzle, T., Mailleux, A. A., Overholtzer, M., Carroll, J. S., Solimini, N. L., Lightcap, E. S., Veiby, O. P., and Brugge, J. S. (2007) *Proc. Natl. Acad. Sci. U.S.A.* **104,** 3787–3792
46. Ghanaat-Pour, H., and Sjöholm, A. (2009) *Diabetes Metab. Res. Rev.* **25,** 163–184
47. Lei, K., and Davis, R. J. (2003) *Proc. Natl. Acad. Sci. U.S.A.* **100,** 2432–2437
48. Memmott, R. M., and Dennis, P. A. (2009) *Cell. Signal.* **21,** 656–664